Catena 223 (2023) 106931

Contents lists available at ScienceDirect

Catena

journal homepage: www.elsevier.com/locate/catena

Age and recurrence of coseismic rock avalanches in Sierra de la Sobia (Cantabrian Mountains, Spain)

Laura Rodríguez-Rodríguez [a,*], Francisco José Fernández [a], Rosana Menéndez-Duarte [a], Valery Guillou [b,1], Beatriz Puente-Berdasco [a], Vincent Rinterknecht [b,1], ASTER Team [b,1]

[a] University of Oviedo, Department of Geology, c/ Jesús Arias de Velasco s/n, 33005 Oviedo, Spain
[b] Aix Marseille Univ., CNRS, IRD, INRA, UM34 CEREGE, Technopôle de l'Environnement Arbois-Méditerranée, BP80, 13545 Aix-en-Provence, France

ARTICLE INFO

Keywords:
Rock avalanche
^{36}Cl CRE dating
Cantabrian Mountains
Paleo-seismicity
Quaternary tectonics

ABSTRACT

Dating of rock avalanche clusters along faults may provide paleo-earthquake data for locations where direct fault-rupture evidence is rare. This study focuses on the rock avalanche cluster preserved in the western slope of Sierra de la Sobia (Cantabrian Mountains, Spain), where evidence of Quaternary faulting was previously reported at the Marabio Fault segment, a splay of the long-lived León Fault. In a previous study we interpret this cluster as seismically induced based on the kinematic analysis of local fault structures, the block size distribution analysis of several rock avalanche accumulation bodies, and the stability analysis of current slopes. In this new study we date these deposits to assess the timing of the recurrent events and evaluate a paleo earthquake record. We determine the ages of 20 boulders from the coarse carapace of two calcareous rock avalanche deposits using the ^{36}Cl Cosmic Ray Exposure dating technique. Our results indicate that the youngest instability event occurred 8.5 ± 0.6 ka ago and was simultaneously recorded by the recent lobes of the two rock avalanches and could correspond to the latest severe earthquake striking this area. The analysis of boulder age clusters in the middle and distal lobes of both rock avalanches reflects up to four additional coseismic instability episodes between ~22.0 and ~10.9 ka, with a recurrence interval of ~3.7 ka on average. Extending this chronological analysis to other rock avalanche clusters could improve our understanding on landscape evolution and its potential for developing regional paleo-earthquake catalogs for the Cantabrian Mountains and other similar contexts.

1. Introduction

Rock avalanches are voluminous, fast-moving slope instabilities that originate when a portion of bedrock falls from a cliff and disintegrates, producing an elongated accumulation of debris with hummocky topography (Hermanns, 2013). Although large (>10^6 m^3) rock avalanches occur infrequently, their size and potential kilometric runout distance make them hazardous in populated mountains and an important process of erosion and sediment delivery to rivers (Croissant et al., 2017; Davies, 2018).

Defining the ultimate trigger responsible for a rock avalanche event is possible in the case of historic events if monitoring data are available (Chang and Taboada, 2009; Yin et al., 2011), but challenging for old rock avalanches as the timing of the event must be determined. The commonest triggers for old rock avalanches referred to in the literature are: (i) intense rainfall events or climatically driven hydrological perturbations (Bayrakdar et al., 2020; Březný et al., 2020; Deplazes et al., 2007; Zerathe et al., 2014); (ii) earthquakes (Grämiger et al., 2016; Lebourg et al., 2014; Nagelisen et al., 2015; Stock and Uhrhammer, 2010); and (iii) stress corrosion or static fatigue of mountain massifs either due to progressive gravitational settlement (Davies, 2018) or linked to glacier retreat (debuttressing) and paraglacial dynamics (Ambrosi and Crosta, 2011; Ballantyne, 2002; Ballantyne et al., 2014; Ballantyne and Stone, 2013; Cossart et al., 2008; McColl, 2012; Mercier et al., 2017). Among these, earthquakes are thought to be responsible for the most voluminous rock avalanches since seismic resonance leads to a deeper propagation of the failure surface compared to aseismic rock avalanches, frequently entailing the topographic lowering of mountain ridgelines (Davies, 2018 and references therein). Furthermore, conceptual and case study analyses have demonstrated that recurrent seismic activity favors progressive fracture propagation and bedrock weakening, ultimately leading to slope failure by seismic fatigue (Gischig et al.,

* Corresponding author.
E-mail address: rodriguezrlaura@uniovi.es (L. Rodríguez-Rodríguez).
[1] [ASTER Team: Georges Aumaître, Karim Keddadouche, Didier Bourlès].

https://doi.org/10.1016/j.catena.2023.106931
Received 7 October 2022; Received in revised form 19 December 2022; Accepted 5 January 2023
Available online 10 January 2023

2016; Zhou et al., 2020). However, the attribution of slope instability initiation to seismic activity is frequently inconclusive or considered unlikely in mountain settings and regions displaying low seismic activity (Hashemi et al., 2022). This is the case of the Pyrenees (Gutiérrez-Santolalla et al., 2005) and the Cantabrian Mountains (Rodríguez-Rodríguez et al., 2018), where tectonic deformation occurs at low to moderate rates and the earthquake record is too limited as to cover the recurrence time of severe earthquakes (Fig. 1). In such scenarios, the spatio-temporal clustering of rock avalanches has been ascribed based on the timing coincidence between rock avalanche dates and climate anomalies. For instance, a peak of deep-seated landslide activity recorded in the western European Alps clustered around 3.3 to 5.1 ka was interpreted as most likely triggered by the 4.2 ka climatic anomaly because the area is outside the reach of Quaternary glaciations and few historic earthquakes approached M > 5 (Zerathe et al., 2014). By contrast, paleoseismic evidence preserved in lacustrine basins in the eastern Alps supports an enhanced seismicity period starting at ~ 7 ka BP, with multiple earthquakes striking the area right before a spatial–temporal rockslide cluster registered at ~ 4.4–3.0 ka BP, henceforth pointing to seismic fatigue as a relevant preparatory factor (Oswald et al., 2021a, 2021b). The most voluminous instabilities recorded in the Alps, the Flims rockslide and the Köfels landslide (Deplazes et al., 2007; Ivy-Ochs et al., 1998), are contemporary and thought to share a common trigger (Nicolussi et al., 2015), possibly seismic (Kremer et al., 2020). This work focuses on the study of recurrent rock avalanche activity preserved in the Cantabrian Mountains (N Iberian Peninsula), where a spatial cluster of rock avalanches has been previously interpreted as coseismic (Fernández et al., 2021). Here we use ^{36}Cl Cosmic Ray Exposure (CRE) dating to date some of these rock avalanches and we explore the usefulness of the dataset as a potential record of past severe earthquakes.

2. Study area

The Cantabrian Mountains is an E-W oriented mountain range uplifted during the Alpine Orogeny and geologically considered the westward continuation of the Pyrenees as a single orogen, since the northward dipping crustal root is continuous beneath the Basque-Cantabrian basin (Pedreira et al., 2007, 2003). The main phase of Alpine exhumation took place in the Cantabrian Mountains between 39 and 29 Ma ago at a rate of 0.24–0.3 km Ma^{-1}, synchronously with the exhumation of the central Pyrenees though at a slower rate (Fillon et al., 2016). Geophysical profiles suggest that the Alpine orogeny entailed a minimum shortening of around 100 km since the Late Cretaceous (Pedreira et al., 2015). The overall structure is interpreted as a monoclinal flexure (Alonso et al., 1996) related to a set of south-verging thrusts dipping 30-36°N, cutting the upper crust in a ramp geometry and rooting at the boundary with the middle crust (Gallastegui et al., 2016). The Paleozoic basement and the Mesozoic cover, both composed

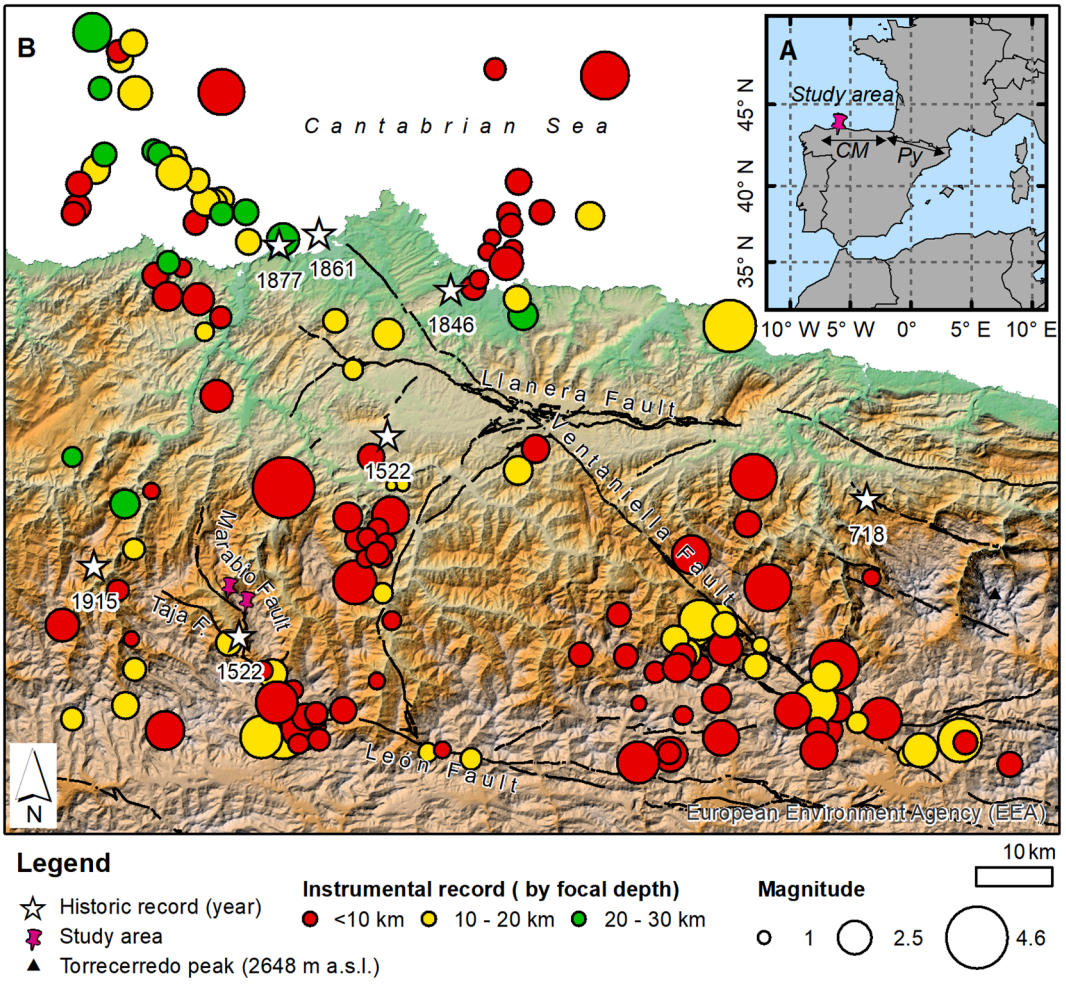

Fig. 1. A) Geographic location of the Cantabrian Mountains (CM) and the Pyrenees (Py) in the context of the Iberian Peninsula. B) Location and seismicity of the study area, Sierra de la Sobia, in the central Cantabrian Mountains. The two rock avalanches analyzed in this work are related to the Marabio Fault segment, located at the western long-lived León Fault tip. The trace of the main active faults during the Alpine cycle is displayed together with available historical (Crespo-Martín et al., 2018; López-Fernández et al., 2018) and instrumental earthquake records (https://www.ign.es/web/ign/portal/sis-catalogo-terremotos, last accessed on June 2022). The base map was taken from the European Environmental Agency (EEA); topographic elevation in inset B range between 0 and 2648 m a.s.l.

of alternations of terrigenous and carbonate sedimentary rocks, remained undetached during the Alpine compression, which was mostly accommodated by tectonic inversion of Mesozoic normal faults (Alonso et al., 1996; Pulgar et al., 1999) and retightening of previous Variscan fold and thrust structures (Alonso et al., 2018). For instance, the long-lived León Fault shelters Cretaceous materials near the Cantabrian mountain range divide, evidence of its reactivation during the Alpine cycle (Alonso et al., 2007).

Though the main episode of Alpine exhumation ceased in the Oligocene (Fillon et al., 2016), the historic and instrumental earthquake records evidence persistent seismic activity driven by the slow WNW-ESE convergence (~5 mm yr^{-1}) between the Nubia and Eurasian tectonic plates (Stich et al., 2020), producing earthquakes of low to moderate magnitude (Crespo-Martín et al., 2018; López-Fernández et al., 2018), rarely exceeding M > 4 (Fig. 1). Most earthquakes occur along the Ventaniella and León faults and particularly at their junction (López-Fernández et al., 2018). In a preliminary analysis, we noted that seventy percent of large-scale slope instabilities documented as either rock avalanches or landslides in the geological map developed by the Spanish Geological Survey are placed at a distance shorter than 5 km from Alpine faults like the long-lived Ventaniella and León faults, suggesting a potential relation between rock avalanche initiation and seismicity (Fig. 2). A possible explanation would be that some of these slope instabilities were seismically induced by severe earthquakes occurring at recurrence intervals longer than the time covered by the instrumental and historic records. Extending this record for longer time intervals would require the analysis of paleoseismic evidence, but outcrops of fault-related Cenozoic sediments are very limited in the Cantabrian Zone. In this regard, evidence of recent tectonic activity is preserved along the Cantabrian coastline, where few inverse faults are affecting both the marine terrace surfaces (locally known as rasas) and their overlaid Quaternary formations (Álvarez-Marrón et al., 2008; Gutiérrez

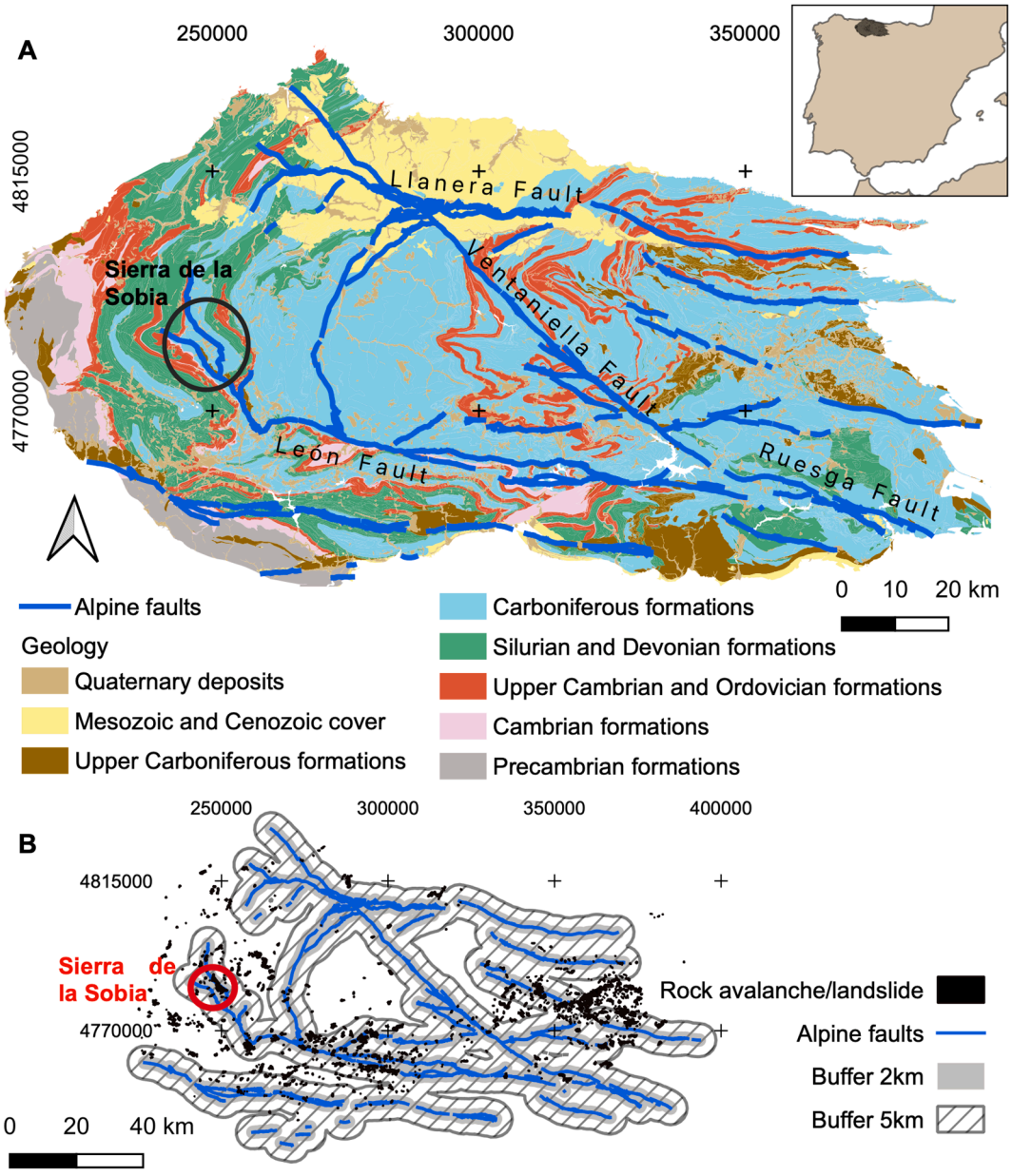

Fig. 2. (A) Geologic map of the Cantabrian Zone based on the continuous GEODE geological map, developed at 1:50,000 scale by the Spanish Geological Survey (Merino-Tomé et al., 2011). Only long-lived faults that were active during the Alpine orogeny are displayed. The inset map shows the location of the Cantabrian Zone in the context of the Iberian Peninsula. (B) Spatial clustering of rock avalanche and landslide deposits inventoried in the GEODE following the trace of Alpine faults. Projection: ETRS89/UTM Zone 30 N.

Claverol et al., 2006). For instance, the Ventaniella Fault causes a vertical offset of 50 m in the elevation of the highest rasa (López-Fernández et al., 2020), and a 2000 km^2 submarine landslide overlaps the underwater continuation of this fault and is attributed to recent seismicity (Fernández-Viejo et al., 2014), but no chronological constraint is available for these paleoseismic records. Similarly, the León Fault has multiple calcareous rock avalanche clusters along its trace.

One cluster is located in Sierra de la Sobia, an arcuate mountain range with a lineation of Carboniferous limestone peaks that increase in elevation southwards from ca. 1300 to 1800 m a.s.l. along more than 12 km, following the trend of the eastern limb of the Sobia Syncline (Menéndez-Duarte and Fernández, 2014). The origin of this rock avalanche cluster has been interpreted as coseismic based on structural and geomorphological data gathered on the western flank of Sierra de la Sobia by Fernández et al. (2021). First, the most voluminous rock avalanches appear along the hinge and southern domains of Sierra de la Sobia where a splitting of the León Fault, named the Marabio Fault, approaches the western hillslope (Fig. 1). The kinematic analysis of minor faults that cut and displace the Marabio Fault trace is consistent with a re-tightening by horizontal shortening according to the current regional NNW maximum horizontal stress (Custódio et al., 2015; de Vicente et al., 2008), causing the stretching of the outer arc of Sierra de la Sobia and the activation of minor faults that accommodate surface deformation. Second, the rock avalanches show accumulation bodies frequently composed by overlapped deposits suggesting their association to multiple instability events, with the oldest deposits partly covered by vegetation and displaying secondary carbonate cements coating the blocks, whereas the youngest deposits are bare of vegetation and non-cemented. The analysis of several rock avalanche accumulation bodies, including the most voluminous ones of Entrago and Carrea ($>3 \times 10^6$ m^3), showed that block-size distribution is not fractal and displays a slope change in the best linear fit of the log frequency - log radius plot at block radius $r_k \sim 1$ m (Fernández et al., 2021). Block sizes with $r_k > 1$ m show a fractal dimension, D, ranging between 2.7 and 2.35, which is into the usual range of dynamic fragmentation described for carbonate cataclasite rocks (Storti et al., 2003). A comparative block-size distribution analysis between the different lobes of the Entrago rock avalanche shows that D seems time-dependent and tends to reduce as the relative age of the deposit increases until it eventually becomes fractal in the earliest deposit. The slope break attenuation observed in the log frequency - log radius plot between the different rock avalanche lobes has been interpreted as resulting from a two-stage breakage: dynamic fragmentation developed at the fault zone (which crosses the rupture scarp in this particular case study) followed by fragmentation by wear and attrition as blocks fall and travel downslope (Fernández et al., 2021). Third, stability analysis of current rupture scars of four different rock avalanches (including those of Entrago and Carrea) indicate that they are stable under static conditions and require a horizontal ground acceleration peak of $>$ 0.10–0.15 g to become unstable, which is within the prediction of the 2013 European Seismic Hazard Map (Giardini et al., 2014). Moreover, unequivocal evidence of Quaternary tectonics has been reported in this area along the Marabio Fault segment, where a reverse fault locally superposes Carboniferous limestone onto cemented talus scree deposits for which a net slip up to 6 m has been estimated (Fernández et al., 2018). A first dating attempt to constraint the age of the oldest rock avalanche deposits was done applying the U-Th technique to the secondary calcite cements coating the blocks. Cement samples could theoretically provide a minimum age constrain for the rock avalanches as long as cement precipitation starts after the slope failure and rock avalanche deposition. Three samples from the oldest lobe of the Entrago rock avalanche yielded ages of 278.3 ± 32.9 ka (RB-6; 12% error), 194.3 ± 70.2 ka (RB-7; 36% error) and 13.7 ± 0.9 ka (RB-5; 7% error), suggesting multiple cementation episodes during Marine Isotope Stages (MIS) 9a, 7a and 1, whereas the oldest lobe of the Carrea rock avalanche yielded two ages of 58.8 ± 14.6 ka (RB-2; 25% error) and 38.3 ± 2.8 ka (RB-9; 7% error) that are coeval to MIS 3 (Fernández et al., 2021). These results suggest that cement precipitation occurs preferentially during Interglacial periods, which are milder and wetter than Glacials periods, in agreement with stalagmite growth patterns observed in several caves of the region (Stoll et al., 2013). However, some samples display large age analytical uncertainties possibly due to the incorporation of detrital Th, which can substantially overestimate the age especially when the host rock has low U content (Fairchild and Baker, 2012). Given these uncertainties, this work aims to refine the available chronological framework by applying ^{36}Cl CRE dating of rock avalanche boulder populations, covering the youngest lobes of the Carrea and Entrago rock avalanches, and the oldest lobe of Entrago, where the greatest age dispersion between U-Th samples is observed. Providing direct age constraint for the latest rock avalanche deposits occurred in the Sierra de la Sobia will give information on the recurrence time of past severe earthquakes striking the region, key to improve seismic risk assessment.

3. Methods

Boulder populations from the coarse carapace of the Entrago and Carrea rock avalanches were targeted for ^{36}Cl CRE dating (Figs. 3 and 4; Table 1). Fifteen samples were collected at the Entrago rock avalanche, evenly distributed to cover the early (LBE1), middle (LBE2) and recent (LBE3) lobes described in Fernández et al. (2021) and Menéndez-Duarte and Fernández (2014). Sampled boulders are located at elevations in the range 461–627 m a.s.l. and runout distances from the head scarp of 867–969 m in the early lobe, 600–679 m in the middle lobe, and 381–450 m in the recent lobe. The boulders sampled in early lobe of Entrago are all located in the area located between the Entrago village and a nearby landfill, where the lobe surface has likely remained 'in situ' (Fig. 5). Additionally, five boulders were sampled at the Carrea rock avalanche (named LBC) located at elevations between 1122 and 1135 m a.s.l. and distributed at runout distances of 424–526 m from the head scarp. The volume of targeted boulders ranges between ~ 10 and 175 m^3, exceptionally overcoming 500 m^3 (Table 1). All sampled boulder lithology corresponds to the Valdeteja Formation, a massively bedded limestone ranging in age between the Bashkirian and early Moscovian (Villa et al., 2001; Wagner et al., 1971). Samples were collected from the top surface of boulders using a hammer and a chisel and GPS positioned. Most sampled boulders displayed flat or nearly flat top surfaces. In the latest case, the dip direction and dip angle of the surface were measured with a compass to correct for self-shielding effects. In addition, horizon readings were taken in the field at each sampling site with a clinometer and a compass to consider topographic shielding effects on exposure age calculations. An average rock density of 2.69 ± 0.03 g cm^{-3} was measured through the Archimedes method for the sampled limestone formation. Finally, the thickness of each sample was measured before the chemical treatment.

Cosmogenic ^{36}Cl is produced from: (i) spallation reactions between secondary cosmic rays with Ca, K, Ti and Fe; (ii) capture of slow negative muons by K and Ca; and (iii) low-energy neutron capture by ^{35}Cl, thus the relative contribution of each reaction will vary depending on target element concentrations in the rock (Schimmelpfennig et al., 2009). Samples were treated at the *Laboratoire National des Nucleides Cosmogéniques* (CEREGE, Aix-en-Provence). First, they were crushed and sieved to select the 250–500 μm fraction for the ^{36}Cl extraction, while the major and trace element composition of the bulk rock were measured using the $<$ 250 μm fraction (Tables 2 and 3). Second, an amount of ~ 100 g per sample was leached in deionized water and then partially (10%) dissolved in nitric acid to remove atmospheric ^{36}Cl (Zreda et al., 1991). Third, each sample was spiked with ~ 0.3 mg of Cl carrier solution with a Cl concentration of 6.92 ± 0.05 mg/g (99.89% ^{35}Cl and 0.11% of ^{37}Cl) and fully dissolved in 2 M HNO_3. Then, an aliquot was taken to determine the concentration of Ca, K and Mg in the target solution by ICP-OES at the *Laboratoire National des Nucleides Cosmogéniques* (Table 4). Finally, samples were mixed with AgCl to

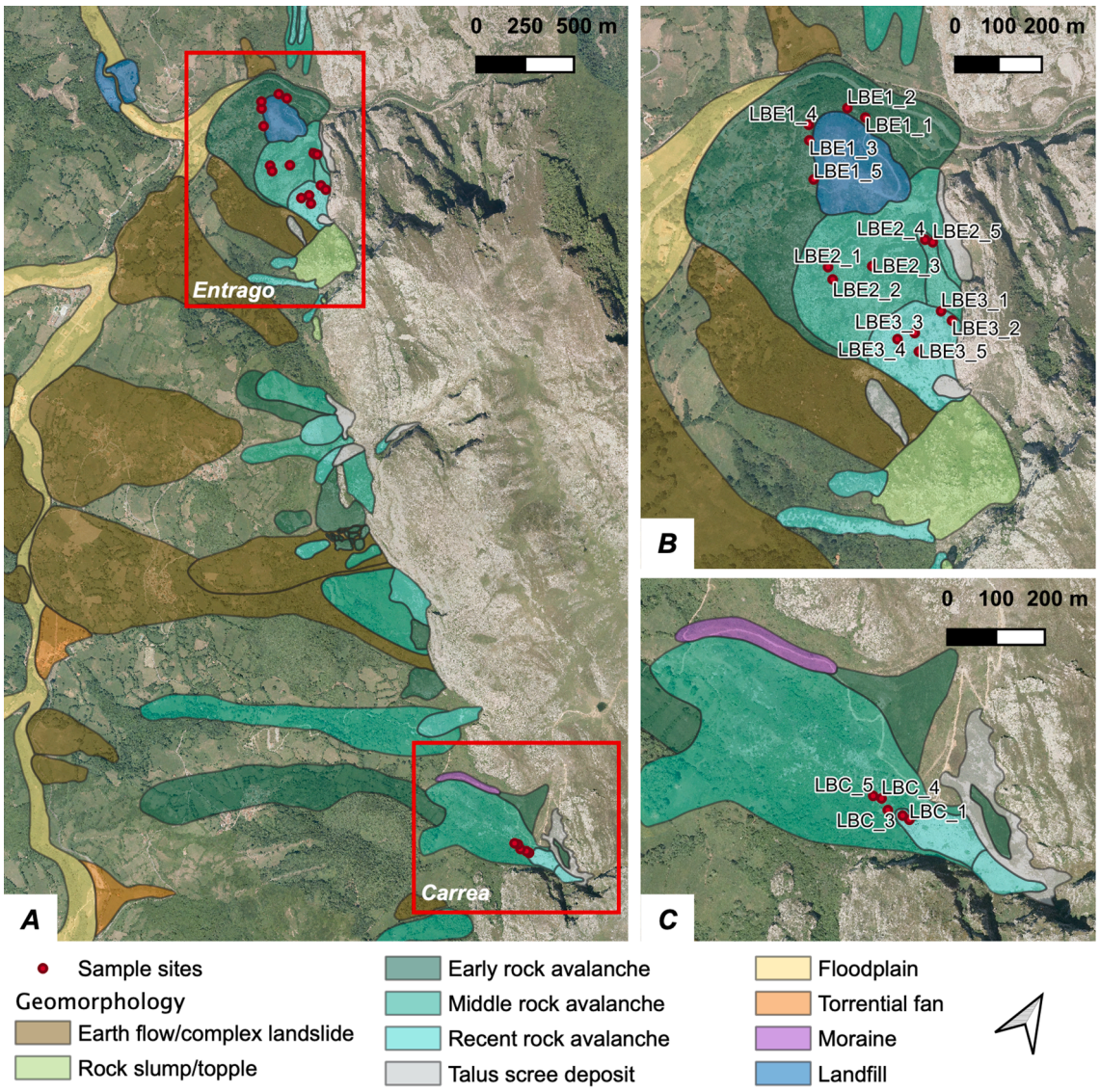

Fig. 3. Rock avalanche and slope instability cluster preserved in the western slope of Sierra de la Sobia: (A) geomorphological map showing the location of the Entrago (B) and Carrea (C) rock avalanches, where multiple boulders were sampled for ^{36}Cl CRE dating. The base information corresponds to the PNOA 2017 orthophotography taken by the Spanish IGN. Geomorphological map was taken from Fernández et al. (2021).

produce targets for Accelerator Mass Spectrometry analysis at the French 5MV accelerator ASTER (CEREGE, Aix-en-Provence). The use of an isotopically enriched carrier allowed a simultaneous measurement of ^{35}Cl/^{37}Cl and the determination of the natural Cl content of dissolved samples. Measured ratios were calibrated against the in-house CEREGE STD standard (Braucher et al., 2018; Merchel et al., 2011), with a given ^{36}Cl/^{35}Cl value of 1.428 ± 0.021 × 10^{-12}.

Boulder ages were calculated using the ^{36}Cl Exposure Age Calculator v2.1 of the CRONUS Earth Web Calculators (Marrero et al., 2016a, 2021), considering the geomagnetically-corrected version of the Lal (1991)/Stone (2000) production rate model, known as the Lm scaling scheme (Marrero et al., 2016b). Boulder exposure ages were calculated for a zero-erosion scenario and corrected for topographic shielding, self-shielding, and thickness effects. The shielding effects of vegetation and snow cover were considered negligible. Although the samples were always collected avoiding the areas with evident post-depositional dissolution, maximum erosion rates were estimated based on surface lowering measurements taken from small-scale karren forms present at the surface of some boulders, mostly circular plan forms like micropits and occasional pans (Ford and Williams, 2007). The maximum surface lowering divided by the minimum boulder exposure age obtained for a zero-erosion scenario provides a maximum estimate for surface erosion. Therefore, boulder age calculations were run again for erosion rate scenarios of 1.9 ± 0.9 mm/ka and 10 ± 3 mm/ka, resulting in age increases by up to 2% and 14 %, respectively, when compared against the zero-erosion scenario, which is the one discussed in the results section.

4. Results

All samples have ^{36}Cl/^{35}Cl ratios between 1.01 × 10^{-12} and 1.72 × 10^{-13} compared to a process blank with a ^{36}Cl/^{35}Cl ratio of 3.11 ± 1.04 × 10^{-15}. The uncertainty of raw AMS data is 1.7–2.9% for the ^{35}Cl/^{37}Cl and 4.1–7.1% for the ^{36}Cl/^{35}Cl. AMS results, calculated ^{36}Cl concentrations, and resultant CRE ages are reported in Table 4 and accompanied by their corresponding one sigma uncertainty (values in brackets include production rate uncertainty).

Boulder ^{36}Cl CRE ages of the Entrago rock avalanche range between 7.8 ± 0.5 ka and 23.6 ± 1.8 ka. Only the recent lobe (LBE-3 samples) shows a well-clustered population of ages pointing to a Holocene rock avalanche event centered at 8.5 ± 0.6 ka, which is also represented by

Fig. 4. Panoramic views of the Entrago (A) and Carrea (B) rock avalanches.

Table 1
Summary of sampled boulders and their characteristics. Samples were collected in May-June 2017. The topographic shielding factor was estimated with the CRONUS Earth topographic shielding calculator (http://cronus.cosmogenicnuclides.rocks/2.1/html/topo/).

Sample	Longitude	Latitude	Elevation	Thickness	Surface	Shielding	Lambda effective	Boulder volume	Runout distance
Id	DD	DD	m	cm	tilt	factor	g cm^{-2}	m^3	m
LBE 1–1	−6.092	43.174	461	4.5	85/13	0.965	151,106	174.6	921
LBE 1–2	−6.093	43.174	464	2.2	Flat	0.965	155,619	135	909
LBE 1–3	−6.093	43.173	475	1.5	Flat	0.967	155,409	39.4	930
LBE 1–4	−6.094	43.173	471	3.0	142/16	0.981	148,478	21.4	969
LBE 1–5	−6.093	43.172	475	2.5	Flat	0.978	154,653	115.9	867
LBE 2–1	−6.091	43.171	521	4.0	Flat	0.986	154,095	41.9	679
LBE 2–2	−6.091	43.170	524	2.0	Flat	0.981	154,499	772.8	655
LBE 2–3	−6.090	43.171	541	1.0	Flat	0.970	155,335	115	618
LBE 2–4	−6.089	43.172	548	2.5	Flat	0.927	157,487	107.5	605
LBE 2–5	−6.089	43.172	550	3.5	Flat	0.924	157,397	12.8	600
LBE 3–1	−6.088	43.171	593	2.0	Flat	0.796	161,411	525	442
LBE 3–2	−6.087	43.171	596	4.3	170/9	0.876	157,240	9.8	416
LBE 3–3	−6.088	43.170	613	3.0	Flat	0.928	157,726	17.9	450
LBE 3–4	−6.088	43.170	601	3.5	195/13	0.937	153,831	74.4	440
LBE 3–5	−6.087	43.170	627	3.5	130/15	0.953	150,134	26.6	381
LBC-1	−6.054	43.150	1135	3.0	346/6	0.921	157,922	19.8	424
LBC-2	−6.054	43.150	1131	3.5	256/6	0.928	159,232	159.3	440
LBC-3	−6.055	43.150	1126	3.0	280/8	0.939	157,626	113.7	472
LBC-4	−6.055	43.150	1124	2.0	200/20	0.946	149,658	40.6	496
LBC-5	−6.055	43.150	1122	3.0	Flat	0.913	159,790	16.7	526

boulder LBE 1–4 in the early lobe. In contrast, the middle (LBE 2 samples) and early (LBE 1 samples) lobes of the Entrago rock avalanche show increasing boulder age scattering accordingly to increasing runout distance from the main scarp (Fig. 6). The youngest boulder of the Entrago middle lobe yields an age of 10.8 ± 0.7 ka and coincides, within one sigma uncertainty, with the age of 11.0 ± 0.7 ka reported for boulder LBE 1–3 in the early lobe. The remaining boulders of the middle lobe group in two clusters centered at 18.0 ± 0.7 and 21.2 ± 0.5 ka, overlapping exposure ages reported for boulders LBE 1–5 and LBE 1–2, respectively. Henceforth, the Entrago rock avalanche dataset is consistent with repeated rock avalanche events resulting in spatially overlapped accumulation bodies, with the youngest event well constrained at 8.5 ka by the boulder age population obtained in the recent lobe.

In the case of the Carrea rock avalanche, boulder CRE ages are bimodally distributed, with the three youngest boulders showing a good correspondence to the 8.5 ka event detected in the recent lobe of the Entrago rock avalanche. In contrast, the two oldest boulders of the Carrea rock avalanche point to a previous event centered around 15.2

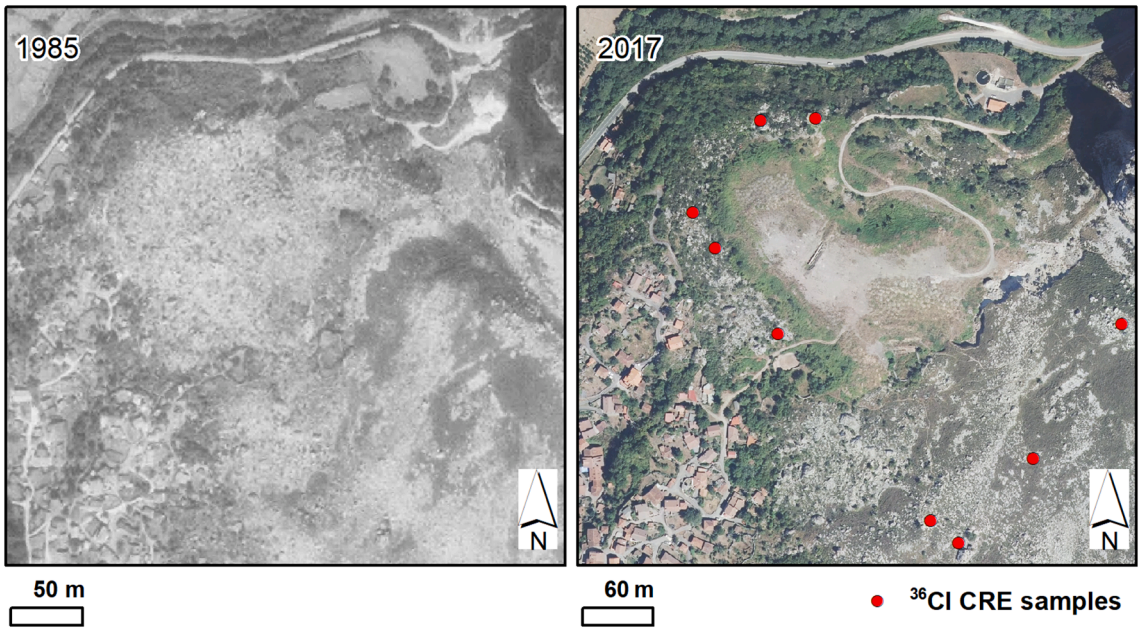

Fig. 5. Aerial photographs of the Entrago early lobe taken in 1985, before the landfill creation, and in 2017 (the year when CRE samples were collected). All CRE samples were taken in the undisturbed areas of the early rock avalanche lobe, which are located between the Entrago village and the landfill.

Table 2
Major element composition of bulk rock samples was analysed through ICP-OES by Service d'Analyse des Roches et Mineraux (SARM, Nancy). Results for samples LBE 1–2, LBE 2–2, and LBC-2 were considered representative for sites LBE 1, LBE2, and LBC respectively, while the average derived from samples LBE 3–4 and 3–5 was considered for boulder samples LBE 3–1 to 3–3 (<L.D., below detection limit).

Sample	SiO_2	Al_2O_3	Fe_2O_3	MnO	MgO	CaO	Na_2O	K_2O	TiO_2	P_2O_5	L.O.I.	H_2O
Id	%	%	%	%	%	%	%	%	%	%	%	%
LBE 1–2	< L.D.	< L.D.	< L.D.	< L.D.	0.85	54.55	< L.D.	< L.D.	< L.D.	< L.D.	43.51	0.41
LBE 2–2	0.07	< L.D.	0.04	< L.D.	0.65	54.57	< L.D.	< L.D.	< L.D.	< L.D.	43.96	0.52
LBE 3–4	0.05	< L.D.	< L.D.	< L.D.	0.44	55.43	< L.D.	< L.D.	< L.D.	< L.D.	43.69	0.36
LBE 3–5	0.05	< L.D.	< L.D.	< L.D.	1.06	54.33	< L.D.	< L.D.	< L.D.	< L.D.	43.89	0.36
LBC-2	0.09	< L.D.	0.02	< L.D.	0.43	55.43	< L.D.	< L.D.	< L.D.	< L.D.	43.69	0.39

Table 3
Trace element composition of bulk rock was measured using ICP-MS at SCTs (Servicios Científico-Técnicos) at the University of Oviedo (Spain). Results for samples LBE 1–2, LBE 2–2, and LBC-2 were considered representative for boulders at sites LBE 1, LBE2, and LBC respectively, while the average compositions derived from samples LBE 3–2, LBE 3–4, and 3–5 were considered representative for boulder samples LBE 3–1 and 3–3.

Sample	Li	B	Sm	Gd	Th	U
Id	ppm	ppm	ppm	ppm	ppm	ppm
LBE 1–2	0.283	0.416	0.016	0.024	0.004	0.551
LBE 2–2	0.121	0.362	0.080	0.117	0.018	0.575
LBE 3–2	0.307	0.624	0.032	0.047	0.011	0.308
LBE 3–4	0.129	0.482	0.024	0.040	0.005	0.820
LBE 3–5	0.109	0.416	0.063	0.100	0.023	0.410
LBC-2	0.128	0.489	0.126	0.174	0.040	0.375

ka, consistently with the age of 14.8 ± 0.8 ka derived from boulder LBE 1–1 in the early lobe of the Entrago rock avalanche.

5. Discussion

The minimum ^{36}Cl CRE ages obtained for the boulder samples taken at the Entrago and Carrea rock avalanche accumulation bodies span the time interval ~ 6.7–23.6 ka, supporting the hypothesis of recurrent rock avalanche activity along the southern slope of Sierra de la Sobia (Fernández et al., 2021, 2019). In the Carrea rock avalanche, the chronologies relying on U-Th and CRE methods agree well since cement precipitation in the oldest lobe predates CRE ages obtained in the recent lobe. However, only one out of three U-Th dates (sample RB-5) from the early lobe of the Entrago rock avalanche post-dates three out of five CRE ages from this lobe (samples LBE 1–1, LBE 1–2 and LBE 1–5). The local discrepancy between methods could be due to age bias affecting one or both dating methods. For instance, the oldest U-Th ages could be biased by the incorporation of detrital Th. According to the literature, this effect is minimized if the analysis focuses on clean samples with a ^{230}Th/^{232}Th ratio greater than 300 (Hellstrom, 2006). Cement samples were crushed to select 'clean' crystals with the help of a binocular magnifier to minimize this source of bias and the sample that provided the highest ^{230}Th/^{232}Th ratio (300 ± 10) was the oldest (RB-06; Fernández et al., 2021). Therefore, U-Th age dispersion likely reflects the long-term evolution of the slope, while cosmogenic nuclides reflect the latest instability events.

Regarding the CRE ages, boulder age dispersion is a remarkable feature of the two studied accumulation bodies, showing in both cases increasing age dispersion towards the toe of the accumulation body (Fig. 6). Age dispersion is frequently documented in rock avalanche deposits and might be due to either inherited cosmogenic nuclides or to the recurring activity of the instability process (e.g. Březný et al., 2020; Martin et al., 2014). In our case study, pre-glacial inheritance is considered unlikely because the source area of boulders lies at elevations mostly below the equilibrium line altitude inferred for the local Last Glacial Maximum in this sector of the Cantabrian Mountains (Pérez-Alberti et al., 2004; Santos-González et al., 2013). Moreover, the highlands present some glacial evidence like a U-shaped valley (Rodríguez-

Table 4
^{36}Cl exposure ages calculated for sampled boulders in the Entrago and Carrea rock avalanches considering the Lm scaling scheme under a zero-erosion scenario (no snow correction applied). Age uncertainty reported in bracket includes production rate uncertainty. Exposure ages calculated using the CRONUS Earth Web Calculators (http://cronus.cosmogenicnuclides.rocks/2.1/html/cl/; last accessed in June 2022).

Sample	Mass of rock dissolved	Mass of Cl in spike	Target				^{36}Cl/^{35}Cl	^{35}Cl/^{37}Cl	m $_{Cl\ nat.}$ /m $_{dissolved.\ rock}$	[^{36}Cl]	Exposure age
			K_2O	CaO	Ti_2O	Fe_2O_3					
Id	g	10^{-3} g	%	%	%	%	10^{-13}		ppm	10^4 at g^{-1}	ka
LBE 1–1	78.530	2.032	0	3.70	0	0	4.849	6.088	35.99 ± 1.42	44.097 ± 2.278	14.8 ± 0.8 (1.2)
LBE 1–2	78.490	2.023	0	3.56	0	0	4.540	4.153	104.19 ± 7.58	81.038 ± 5.997	23.6 ± 1.8 (2.7)
LBE 1–3	79.325	2.015	0	3.66	0	0	3.480	5.630	41.86 ± 1.72	33.947 ± 1.888	11.0 ± 0.6 (1.0)
LBE 1–4	81.495	2.046	0	3.87	0	0	2.898	5.416	45.26 ± 1.97	29.364 ± 1.714	9.3 ± 0.6 (0.9)
LBE 1–5	78.585	2.043	0	3.68	0	0	5.793	5.591	43.53 ± 1.83	58.446 ± 2.979	18.8 ± 0.9 (1.5)
LBE 2–1	78.070	2039	0	3.56	0	0	6.644	5.351	48.51 ± 2.12	71.448 ± 3.635	21.6 ± 1.1 (1.8)
LBE 2–2	79.175	2.028	0	3.70	0	0	3.150	5.047	55.13 ± 2.68	36.210 ± 2.227	10.8 ± 0.7 (1.0)
LBE 2–3	70.650	2.042	0	3.51	0	0	7.177	6.609	34.11 ± 1.22	67.342 ± 3.138	20.9 ± 1.0 (1.6)
LBE 2–4	53.725	2.035	0	2.69	0	0	5.657	10.283	21.44 ± 0.67	52.586 ± 2.299	17.5 ± 0.8 (1.3)
LBE 2–5	78.010	2.034	0	3.66	0	0	8.553	10.578	14.16 ± 0.39	54.148 ± 2.304	18.5 ± 0.8 (1.4)
LBE 3–1	77.170	2.026	0	3.56	0	0	2.760	5.995	37.71 ± 1.44	25.829 ± 1.515	9.1 ± 0.6 (0.8)
LBE 3–2	81.100	2.028	0	3.70	0	0	1.716	4.134	103.02 ± 7.73	30.068 ± 2.746	8.4 ± 0.8 (1.1)
LBE 3–3	79.055	2.049	0	3.62	0	0	2.649	5.406	46.95 ± 2.12	27.780 ± 1.704	8.1 ± 0.5 (0.8)
LBE 3–4	78.795	2.035	0	3.65	0	0	2.480	5.249	50.27 ± 2.33	27.017 ± 1.759	7.8 ± 0.5 (0.7)
LBE 3–5	79.295	2.024	0	3.59	0	0	2.511	4.721	66.29 ± 3.76	32.412 ± 2.303	8.9 ± 0.7 (0.9)
LBC-1	78.460	2.033	0	3.60	0	0	4.869	8.996	17.97 ± 0.61	33.015 ± 1.543	6.7 ± 0.3 (0.5)
LBC-2	77.215	2.036	0	3.55	0	0	3.215	4.633	72.48 ± 3.99	44.554 ± 2.865	8.1 ± 0.5 (0.8)
LBC-3	81.300	2.039	0	3.76	0	0	4.926	5.653	40.95 ± 1.70	47.254 ± 2.470	9.1 ± 0.5 (0.8)
LBC-4	79.490	2.043	0	3.76	0	0	7.538	5.688	41.39 ± 1.75	73.624 ± 3.640	14.3 ± 0.7 (1.2)
LBC-5	80.030	2.025	0	3.77	0	0	10.139	7.169	25.66 ± 1.38	77.864 ± 3.769	16.2 ± 0.8 (1.3)

Pérez, 2012) and a lateral moraine was found next to the Carrea rock avalanche during the course of our research (Fig. 3C and 4B). In the absence of specific studies on the glacial record of Sierra de la Sobia and considering both the local relief configuration and the ELA estimations previously mentioned, our hypothesis is that a small ice cap drained by short glacier tongues (fronts around 1000 m a.s.l) could have once occupied the highlands of this mountain range. Ice cap glaciers developed on a flattened mountain range would be particularly sensitive to an ELA rise at the end of a glacial cycle, likely recording a fast recession in response to deglaciation. Consequently, glacial erosion could have had contributed to remove any pre-glacial inherited ^{36}Cl from the highlands, which margins are the source area of rock avalanche boulders. Regarding post-glacial inheritance, it could contribute to boulder age dispersion if the sampled surface was already exposed as part of the headwall scarp before the rock avalanche occurred or if it was created by dynamic fragmentation close to the original headwall surface, which is probable in the case of surficial small rock falls but unlikely for voluminous rock avalanches. Therefore, we favor that age dispersion is most likely related to repeated rock avalanche events triggered by earthquakes, eventually resulting in spatially overlapped accumulation deposits. Boulder ages are tightly grouped for short runout distances, where dynamic and ballistic fragmentation are dominant. In those areas the expansion of materials is confined in a smaller area, increasing the odds of sampling boulders from the most recent rock avalanche event. In contrast, age dispersion rises towards the rock avalanche toe in the same direction that block size distribution is increasingly influenced by wear and attrition as dominant fragmentation processes during the motion of the avalanche (Fernández et al., 2021). The idea that the old lobes might have some younger boulders due to more recent events is supported by previous evidence documented in the Villa de Sub rock avalanche, in the southern sector of Sierra de la Sobia (5 km south from the Carrea rock avalanche), where the coseismic rock falls occurred in 1996 and 2004 have incorporated some isolated boulders to the middle and recent lobes of the rock avalanche (Fernández et al., 2021; Menéndez-Duarte and Fernández, 2014). Moreover, previous works in the literature have shown that the topographic configuration of the site can also enhance seismic shaking (Khajavi et al., 2012), eventually leading to slope instability. Also, it has been documented that landslide body sediments can record shaking amplification during earthquakes due to low shear wave velocities relative to the surrounding intact rock slopes (Moore et al., 2011). Similarly, boulders in a rock avalanche accumulation body could be overturned, dislodged, and even roll downslope under the influence of high seismic shaking intensities. Most of the boulders sampled are massive reducing this possibility (see Table 1 and Fig. 6).

Only the five boulders sampled at the recent lobe of the Entrago rock avalanche provide a normally distributed age population centered at 8.5 ± 0.6 ka and coincides with the ages obtained in three out of five boulders sampled at the Carrea rock avalanche. Hence, an important

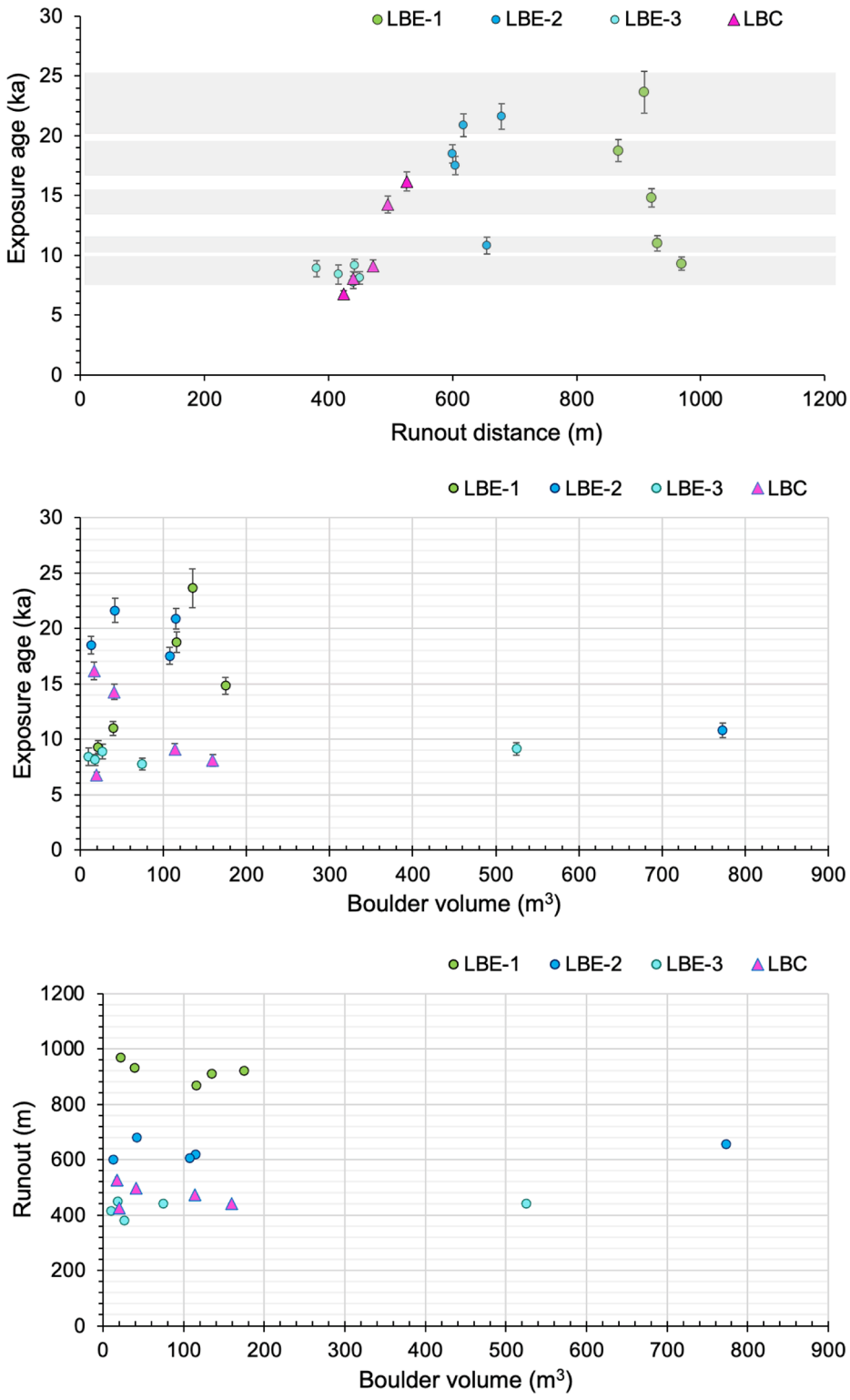

Fig. 6. Boulder exposure ages of the Entrago and Carrea rock avalanches show an increase in age dispersion when increasing runout distance from the depletion areas. Only the recent lobe of the Entrago rock avalanche (LBE-3) provides a well-clustered age population centered at ~ 8.5 ka. Grey bands in the upper graph indicate overlapping ages within its one sigma error.

instability episode can be placed around 8.5 ka with confidence, coinciding within age uncertainty with the 8.2 ka event, a short-lived cooling episode initiated by a perturbation of the ocean thermohaline circulation in response to the catastrophic drainage of proglacial lakes Agassiz and Ojibway into the Atlantic Ocean (Barber et al., 1999; Matero et al., 2017; Thomas et al., 2007). Stalagmite records from the Cantabrian Mountains document two $\delta^{18}O$ excursions attributed to cooler sea surface temperatures during the 8.2 ka event (Dominguez-Villar et al., 2009), resulting in cooler winters, drier summers, and enhanced seasonality (Baldini et al., 2019), changes that could have affected the hydrological condition of slopes and their stability (Borgatti and Soldati, 2010). A previous study in the eastern end of the Cantabrian Mountains

has also reported a spatio-temporal cluster of landslides in the Magdalena valley at 8.5–7.5 ka BP, which the authors interpret as potentially related to the 8.2 ka climate anomaly (González-Díez et al., 1996).

Although we do not dismiss the role of climate as a conditioning factor, the fact that the destabilization of the southern slope of La Sobia range occurred at least in two different spots located ~ 3.5 km apart along the trace of the Marabio Fault segment, which has evidence of Quaternary activity (Fernández et al., 2018), strongly points to a seismic trigger. Moreover, there is documented evidence of coseismic rock slope failures within the region. For example the latest instability events corresponded to small rock falls recorded in 1996 and 2004 at the Villa de Sub rock avalanche area synchronously with earthquakes of magnitudes 4.1 and 2, respectively (Fernández et al., 2021; Menéndez-Duarte and Fernández, 2014). The activity along the Marabio fault zone could have contributed to slope destabilization in different ways, such as modifying the topography of the fault scarp from which instabilities fall and contributing to joint propagation and rock mass weakening. Both factors can create seismic site effects that could potentially amplify shaking along the scarp zone contributing to slope destabilization. Joint propagation and dynamic fragmentation occurring along the fault zone also facilitate weathering processes (e.g., gelifraction process during cold climate episodes) that further enhance rock mass weakening through time. Previous slope stability analysis suggests that horizontal peak ground acceleration should reach values of > 0.1 to 0.15 g to drop the slope security factor below 1 (Fernández et al., 2021). For a recurrence interval of 500 years, such ground acceleration value is solely foreseen for the Axial Zone of the Pyrenees and the Betic range in the seismic hazard map of the Spanish IGN (http://www.ign.es/web/resources/sismologia/www/dir_images_terremotos/mapas_sismicidad/peligrosidadaceleracion.jpg; last accessed on July 2022), but higher ground accelerations are expected for longer recurrence intervals (Villamor et al., 2012). In fact, there is a growing body of evidence that mass movement activity could be related to recurrent strong magnitude earthquakes. For instance, in the Pyrenees, Gutiérrez et al. (2008) studied sackung scarps located close to the epicenter of the Mw 5.3 Vielha earthquake occurred in 1923. They found that these landforms are spatially related to the North Maladeta Fault and cite sedimentological evidence of episodic displacement of millennial recurrence (~5.6 ka). These authors consider the sackung scarps and their related sag lake sequences as archives of more severe earthquakes striking the area that are useful for seismic risk assessment as they help to extend the available earthquake catalog. In the Cantabrian Mountains, antislope scarp evidence placed close to the mountain divide has been also documented in the western part of the range, more specifically in the headwaters of the Navia, Narcea and Sil valleys (Alonso and Corte, 1992) and could be related to recent, either post-glacial or Holocene, tectonic activity (though no precise age control is yet available).

Considering that the studied rock avalanche accumulation bodies are composite deposits originated by repeated rock avalanche events likely coseismic (Fernández et al., 2021), the kernel density function obtained for the entire population of boulders might provide insights into the recurrence time of previous severe past earthquakes striking the study area. The kernel density function for the entire boulder population is shown in Fig. 7. The most pronounced peak corresponds to the 8.5 ka event recorded at the upper part of the Entrago and Carrea rock avalanches, and likely reflects the timing of the most recent severe earthquake striking the study area. Meanwhile, boulder ages in the intermediate and distal parts of the analyzed rock avalanches form at least four age clusters centered at minimum exposure ages of 22.0 ± 1.4 ka, 18.2 ± 0.6 ka, 14.5 ± 0.4 ka, and 10.9 ± 0.1 ka, that are roughly spaced in time by ~ 3.7 ka on average for a zero-erosion scenario. Hence, the available data suggests that the last severe earthquake striking the area likely took place in the early Holocene and that the recurrence interval of severe earthquakes is presumably of a few millennia. A preliminary analysis on the contribution of slow slip faults to the seismic hazard of the Iberian Peninsula by Villamor et al. (2012) includes the analysis of the León Fault. Considering a slip rate ranging between 0.1 and 0.01 mm/a, severe earthquakes (Mw ranging between 6.80 and 7.34) could occur along the León Fault at inferred recurrence intervals ranging between 240 and 2.6 ka. Our results considerably narrow the preliminary recurrence interval estimations provided for severe earthquakes along the León Fault provided by Villamor et al. (2012) and confirms that local seismicity can potentially contribute to seismic hazard of critical facilities such as nuclear power plants, dams, or emergency response buildings.

6. Conclusions

The spatial cluster of rock avalanches preserved along the southern slope of Sierra de la Sobia has been dated using ^{36}Cl CRE, providing insights into the timing and temporal recurrence of coseismic instability events potentially linked to the reactivation of the León Fault by

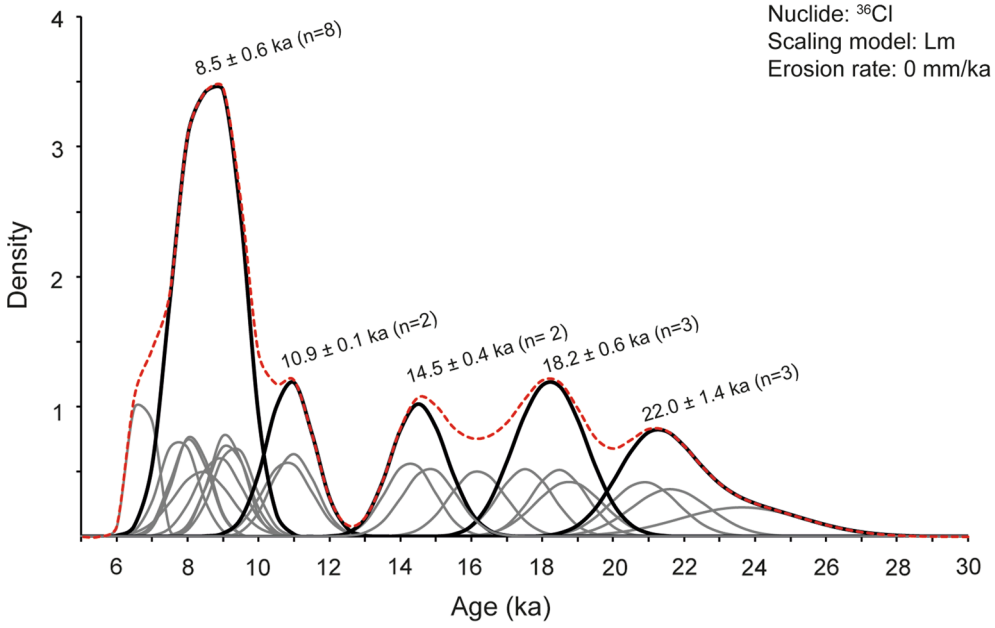

Fig. 7. Kernel density function for the entire boulder population. Considering that repeated rock slope instabilities will lead to composite rock avalanche accumulation bodies with increasing age dispersion towards the foot of the deposit, a kernel density function was constructed considering the entire boulder population sampled at the Entrago and Carrea rock avalanches and represented by the red dashed line, while grey continuous lines reflect each boulder age. The kernel density function of the entire population allows the identification of five boulder age clusters, represented by continuous black lines, which could reflect the latest rock avalanche events striking the study area. The most recent one took place 8.5 ka ago and is preserved at the proximal end of the Entrago and Carrea rock avalanches. (For interpretation of the references to colour in this figure legend, the reader is referred to the web version of this article.)

retightening of the Cantabrian Arc under NNW-SSE compression (Fernández et al., 2021):

1) The most recent instability event was simultaneously recorded at ~ 8.5 ka in the uppermost end of the Carrea and Entrago rock avalanches. They are separated ~ 3.5 km and both placed on the trace of the Marabio fault segment, a splay at the western León Fault tip. This event could correspond to slip on the León Fault and one of the latest severe earthquakes striking the study area.
2) Boulder age dispersion increases towards the rock avalanche toe likely due to the superimposition of rock avalanche accumulation bodies related to different coseismic events.
3) The analysis of boulder age clusters suggests the possibility of four former coseismic instability episodes at ~ 22.0 ka, ~18.2 ka, ~14.5 ka, and ~ 10.9 ka, with a recurrence interval of a few millennia (~3.7 ka on average).

Detailed multivariate analysis and chronological studies should be extended to similar rock avalanche clusters preserved along the long-lived León Fault and other alpine structures of the Cantabrian Mountains, as they offer a unique opportunity to broaden the paleo-earthquake catalog and improve seismic hazard assessment in areas where the Paleozoic basement is directly exposed and clear neotectonic evidence is rare.

Declaration of Competing Interest

The authors declare that they have no known competing financial interests or personal relationships that could have appeared to influence the work reported in this paper.

Data availability

No data was used for the research described in the article.

Acknowledgments

This research has been funded by the Spanish Ministry of Science and Innovation (Projects: CGL2015-66997-R and PID2021-126357NB-100), and by the European Regional Development Fund (FEDER) and Plan de Ciencia Tecnología e Innovación del Principado de Asturias (PCTI) (Grant reference: FC-GRUPIN-IBI/2018/00076/040). The ASTER AMS national facility (CEREGE, Aix-en-Provence) is supported by the INSU/CNRS, the ANR through the "Projets thématiques d'excellence" program for the "Equipements d'excellence" ASTER- CEREGE action and IRD. We are grateful to Samuel McColl for his constructive comments and suggestions during the review process, which help us to improve the original version of the manuscript.

References

Alonso, J.L., Barrón, E., González Fernández, B., Menéndez Casares, E., 2018. Presencia de una sucesión paleógena cobijada por el cabalgamiento de La Espina (límite entre las zonas Cantábrica y Asturoccidental-Leonesa). Implicaciones tectónicas. Geogaceta 64, 11–14.

Alonso, J.L., Martínez-Abad, I., García-Ramos, J.C., 2007. Nota sobre la presencia de una sucesión cretácica en el Macizo de Las Ubiñas (Cordillera Cantábrica). Implicaciones tectónicas y geomorfológicas. Geogaceta 43, 47–50.

Alonso, J.L., Pulgar, J.A., García-Ramos, J.C., Barba, P., 1996. Tertiary basins and Alpine tectonics in the Cantabrian Mountains (NW Spain). In: Friend, P., Dabrios, C. (Eds.), Tertiary Basins of Spain: The Stratigraphic Record of Crustal Kinematics. Cambridge University Press, Cambridge, pp. 214–227.

Alonso, V., Corte, A.E., 1992. Postglacial fracturing in the Cantabrian Cordillera (NW Spain). Z. Geomorph. N.F. 36, 479–490.

Álvarez-Marrón, J., Hetzel, R., Niedermann, S., Menéndez, R., Marquínez, J., 2008. Origin, structure and exposure history of a wave-cut platform more than 1 Ma in age at the coast of northern Spain: A multiple cosmogenic nuclide approach. Geomorphology 93, 316–334. https://doi.org/10.1016/j.geomorph.2007.03.005.

Ambrosi, C., Crosta, G.B., 2011. Valley shape influence on deformation mechanisms of rock slopes. Geol. Soc. London, Spec. Publ. 351, 215 LP – 233 10.1144/SP351.12.

Baldini, L.M., Baldini, J.U.L., McDermott, F., Arias, P., Cueto, M., Fairchild, I.J., Hoffmann, D.L., Mattey, D.P., Müller, W., Nita, D.C., Ontañón, R., Garciá-Moncó, C., Richards, D.A., 2019. North Iberian temperature and rainfall seasonality over the Younger Dryas and Holocene. Quat. Sci. Rev. 226 https://doi.org/10.1016/j.quascirev.2019.105998.

Ballantyne, C.K., 2002. Paraglacial geomorphology. Quat. Sci. Rev. 21, 1935–2017. https://doi.org/10.1016/S0277-3791(02)00005-7.

Ballantyne, C.K., Sandeman, G.F., Stone, J.O., Wilson, P., 2014. Rock-slope failure following Late Pleistocene deglaciation on tectonically stable mountainous terrain. Quat. Sci. Rev. 86, 144–157. https://doi.org/10.1016/j.quascirev.2013.12.021.

Ballantyne, C.K., Stone, J.O., 2013. Timing and periodicity of paraglacial rock-slope failures in the Scottish Highlands. Geomorphology 186, 150–161. https://doi.org/10.1016/j.geomorph.2012.12.030.

Barber, D.C., Dyke, A., Hillaire-Marcel, C., Jennings, A.E., Andrews, J.T., Kerwin, M.W., Bilodeau, G., McNeely, R., Southon, J., Morehead, M.D., Gagnon, J.M., 1999. Forcing of the cold event of 8,200 years ago by catastrophic drainage of Laurentide lakes. Nature 400, 344–348. https://doi.org/10.1038/22504.

Bayrakdar, C., Gorum, T., Çılğın, Z., Vockenhuber, C., Ivy-Ochs, S., Akçar, N., 2020. Chronology and Geomorphological Activity of the Akdag Rock Avalanche (SW Turkey). Front. Earth Sci. 8, 1–20. https://doi.org/10.3389/feart.2020.00295.

Borgatti, L., Soldati, M., 2010. Landslides as a geomorphological proxy for climate change: A record from the Dolomites (northern Italy). Geomorphology 120, 56–64. https://doi.org/10.1016/j.geomorph.2009.09.015.

Braucher, R., Keddadouche, K., Aumaître, G., Bourlès, D.L., Arnold, M., Pivot, S., Baroni, M., Scharf, A., Rugel, G., Bard, E., 2018. Chlorine measurements at the 5MV French AMS national facility ASTER: Associated external uncertainties and comparability with the 6MV DREAMS facility. Nucl. Instruments Methods Phys. Res. Sect B Beam Interact. Mater. Atoms 420, 40–45. https://doi.org/10.1016/j.nimb.2018.01.025.

Břežný, M., Pánek, T., Braucher, R., Šilhán, K., Chalupa, V., Lenart, J., Táborík, P., Team, A., 2020. Old but still active: > 18 ka history of rock slope failures affecting a flysch anticline. Landslides. https://doi.org/10.1007/s10346-020-01483-7.

Chang, K.J., Taboada, A., 2009. Discrete element simulation of the Jiufengershan rock-and-soil avalanche triggered by the 1999 Chi-Chi earthquake, Taiwan. J. Geophys. Res. Earth Surf. 114, F03003. https://doi.org/10.1029/2008JF001075.

Cossart, E., Braucher, R., Fort, M., Bourlès, D.L., Carcaillet, J., 2008. Slope instability in relation to glacial debuttressing in alpine areas (Upper Durance catchment, southeastern France): Evidence from field data and 10Be cosmic ray exposure ages. Geomorphology 95, 3–26. https://doi.org/10.1016/j.geomorph.2006.12.022.

Crespo-Martín, C., Martín-González, F., Lozano, G., 2018. Revisión y ampliación del catálogo sísmico del noroeste de la Península Ibérica previo a 1755 y sus implicaciones en la actividad intraplaca. Estud. Geológicos 74, 085. https://doi.org/10.3989/egeol.43083.477.

Croissant, T., Lague, D., Steer, P., Davy, P., 2017. Rapid post-seismic landslide evacuation boosted by dynamic river width. Nat. Geosci. 10, 680–684. https://doi.org/10.1038/ngeo3005.

Custódio, S., Dias, N.A., Carrilho, F., Góngora, E., Rio, I., Marreiros, C., Morais, I., Alves, P., Matias, L., 2015. Earthquakes in western Iberia: Improving the understanding of lithospheric deformation in a slowly deforming region. Geophys. J. Int. 203, 127–145. https://doi.org/10.1093/gji/ggv285.

Davies, T., 2018. Rock Avalanches. In: Oxford Research Encyclopedia of Natural Hazard Science. Oxford University Press, p. 58. https://doi.org/10.1093/acrefore/9780199389407.013.326.

de Vicente, G., Cloetingh, S., Muñoz-Martín, A., Olaiz, A., Stich, D., Vegas, R., Galindo-Zaldívar, J., Fernández-Lozano, J., 2008. Inversion of moment tensor focal mechanisms for active stresses around the microcontinent Iberia: Tectonic implications. Tectonics 27, 1–22. https://doi.org/10.1029/2006TC002093.

Deplazes, G., Anselmetti, F.S., Hajdas, I., 2007. Lake sediments deposited on the Flims rockslide mass: The key to date the largest mass movement of the Alps. Terra Nov. 19, 252–258. https://doi.org/10.1111/j.1365-3121.2007.00743.x.

Dominguez-Villar, D., Fairchild, I.J., Baker, A., Wang, X., Edwards, R.L., Cheng, H., 2009. Oxygen isotope precipitation anomaly in the North Atlantic region during the 8.2 ka event. Geology 37, 1095–1098. https://doi.org/10.1130/G30393A.1.

Fairchild, I.J., Baker, A., 2012. Dating of Speleothems. In: Speleothem Science. From Process to Past Environments. Wiley-Blackwell, Oxford, pp. 290–301.

Fernández-Viejo, G., López-Fernández, C., Domínguez-Cuesta, M., Cadenas, P., 2014. How much confidence can be conferred on tectonic maps of continental shelves? the Cantabrian-Fault case. Sci. Rep. 4, 1–7. https://doi.org/10.1038/srep03661.

Fernández, F.J., Alonso, J.L., Pando, L., 2018. Evidence for quaternary tectonic activity in the western cantabrian Zone (Passes of Marabio, Sobia nappe). Geogaceta 64, 1–3.

Fernández, F.J., Menéndez-Duarte, R., Pando, L., Rodríguez-Rodríguez, L., Iglesias, M., 2021. Gravitational slope processes triggered by past earthquakes on the Western Cantabrian Mountains (Sierra de la Sobia, Northern Spain). Geomorphology 390, 107867. https://doi.org/10.1016/j.geomorph.2021.107867.

Fernández, F.J., Menéndez-Duarte, R., Rodríguez-Rodríguez, L., Iglesias, M., Pando, L., 2019. Reapretamiento Cuaternario del Arco Cantábrico en el Manto de La Sobia (Zona Cantábrica, NO de España). In: Libro de Resúmenes de La XV Reunión Nacional de Cuaternario. Asociación Española para el Estudio del Cuaternario, Bilbao, pp. 442–445.

Fillon, C., Pedreira, D., Van Der Beek, P.A., Huismans, R.S., Barbero, L., Pulgar, J.A., 2016. Alpine exhumation of the central Cantabrian Mountains, Northwest Spain. Tectonics 35, 339–356. https://doi.org/10.1002/2015TC004050.

Ford, D., Williams, P., 2007. Karst Hydrogeology and Geomorphology. John Wiley & Sons Ltd.

Gallastegui, J., Pulgar, J.A., Gallart, J., 2016. Alpine tectonic wedging and crustal delamination in the Cantabrian Mountains (NW Spain). Solid Earth 7, 1043–1057. https://doi.org/10.5194/se-7-1043-2016.
Giardini, D., Wössner, J., Danciu, L., 2014. Mapping Europe's Seismic Hazard. EOS. Tansactions. Am. Geophys. Union 95, 261–268. https://doi.org/10.1002/2014EO290001.
Gischig, V., Preisig, G., Eberhardt, E., 2016. Numerical investigation of seismically induced rock mass fatigue as a mechanism contributing to the progressive failure of deep-seated landslides. Rock Mech. Rock Eng. 49, 2457–2478.
González-Díez, A., Salas, L., Díaz de Terán, J.R., Cendrero, A., 1996. Late Quaternary climate changes and mass movement frequency and magnitude in the Cantabrian region, Spain. Geomorphology 15, 291–309.
Grämiger, L.M., Moore, J.R., Vockenhuber, C., Aaron, J., Hajdas, I., Ivy-Ochs, S., 2016. Two early Holocene rock avalanches in the Bernese Alps (Rinderhorn, Switzerland). Geomorphology 268, 207–221. https://doi.org/10.1016/j.geomorph.2016.06.008.
Gutiérrez-Santolalla, F., Acosta, E., Ríos, S., Guerrero, J., Lucha, P., 2005. Geomorphology and geochronology of sackung features (uphill-facing scarps) in the Central Spanish Pyrenees. Geomorphology 69, 298–314. https://doi.org/10.1016/j.geomorph.2005.01.012.
Gutiérrez Claverol, M., López Fernández, C., Alonso Alonso, J., 2006. Procesos neotectónicos en los depósitos de rasa en la zona de Canero (Occidente de Asturias). Geogaceta 75–78.
Gutiérrez, F., Ortuño, M., Lucha, P., Guerrero, J., Acosta, E., Coratza, P., Piacentini, D., Soldati, M., 2008. Late Quaternary episodic displacement on a sackung scarp in the central Spanish Pyrenees. Secondary paleoseismic evidence? Geodin. Acta 21, 187–202. https://doi.org/10.3166/ga.21.187-202.
Hashemi, K., Sarikaya, M.A., Görüm, T., Wilcken, K.M., Çiner, A., Žebre, M., Stepišnik, U., Yıldırım, C., 2022. The Namaras rock avalanche: Evidence of mid-to-late Holocene paraglacial activity in the Central Taurus Mountains, SW Turkey. Geomorphology 408, 108261. https://doi.org/10.1016/j.geomorph.2022.108261.
Hellstrom, J., 2006. U-Th dating of speleothem with high initial 230-Th using stratigraphic constraint. Quat. Geochronol. 1, 289–295.
Hermanns, R.L., 2013. Encyclopedia of. Nat. Hazards. https://doi.org/10.1007/978-1-4020-4399-4.
Ivy-Ochs, S., Heuberger, H., Kubik, P.W., Kerschner, H., Bonani, G., Frank, M., Schlüchter, C., 1998. The age of the Köfels event. Relative, 14C and cosmogenic isotope dating of an early Holocene landslide in the central Alps (Tyrol, Austria). Zeitschrift für Gletscherkd. und Glazialgeol. 34, 57–68.
Khajavi, N., Quigley, M., McColl, S.T., Rezanejad, A., 2012. Seismically induced boulder displacement in the Port Hills, New Zealand during the 2010 Darfield (Canterbury) earthquake. New Zeal. J. Geol. Geophys. 55, 271–278. https://doi.org/10.1080/00288306.2012.698627.
Kremer, K., Gassner-Stamm, G., Grolimund, R., Wirth, S.B., Strasser, M., Fäh, D., 2020. A database of potential paleoseismic evidence in Switzerland. J. Seismol. 24, 247–262. https://doi.org/10.1007/s10950-020-09908-5.
Lal, D., 1991. Cosmic ray labeling of erosion surfaces: in situ nuclide production rates and erosion models. Earth Planet. Sci. Lett. 104, 424–439.
Lebourg, T., Zerathe, S., Fabre, R., Giuliano, J., Vidal, M., 2014. A Late Holocene deep-seated landslide in the northern French Pyrenees. Geomorphology 208, 1–10. https://doi.org/10.1016/j.geomorph.2013.11.008.
López-Fernández, C., Llana-Fúnez, S., Fernández-Viejo, G., Domínguez-Cuesta, M.J., Díaz-Díaz, L.M., 2020. Comprehensive characterization of elevated coastal platforms in the north Iberian margin: A new template to quantify uplift rates and tectonic patterns. Geomorphology 364, 107242. https://doi.org/10.1016/j.geomorph.2020.107242.
López-Fernández, C., Fernández-Viejo, G., Olona, J., Llana-Fúnez, S., 2018. Intraplate Seismicity in Northwest Iberia along the Trace of the Ventaniella Fault: A Case for Fault Intersection at Depth. Bull. Seismol. Soc. Am. 108, 604–618. https://doi.org/10.1785/0120170215.
Marrero, S., Phillips, F., Borchers, B., Lifton, N., Aumer, R., Balco, G., 2016a. Cosmogenic nuclide systematics and the CRONUScalc program. Quat. Geochronol. 31, 160–187.
Marrero, S., Phillips, F., Caffee, M., Gosse, J., 2016b. CRONUS-Earth cosmogenic 36Cl calibration. Quat. Geochronol. 31, 199–219.
Marrero, S.M., Phillips, F.M., Caffee, M., Gosse, J., 2021. Corrigendum to "CRONUS-Earth cosmogenic 36Cl calibration"[Quat. Geochronol. 31 (2016) 199–219] (CRONUS-Earth cosmogenic ^3^6Cl calibration (2016) 31 (199–219), (S1871101415300649), (10.1016/j.quageo.2015.10.002)). Quat. Geochronol. 61, 101130. https://doi.org/10.1016/j.quageo.2020.101130.
Martin, S., Campedel, P., Ivy-Ochs, S., Viganò, A., Alfimov, V., Vockenhuber, C., Andreotti, E., Carugati, G., Pasqual, D., Rigo, M., 2014. Lavini di Marco (Trentino, Italy): 36Cl exposure dating of a polyphase rock avalanche. Quat. Geochronol. 19, 106–116. https://doi.org/10.1016/j.quageo.2013.08.003.
Matero, I.S.O., Gregoire, L.J., Ivanovic, R.F., Tindall, J.C., Haywood, A.M., 2017. The 8.2 ka cooling event caused by Laurentide ice saddle collapse. Earth Planet. Sci. Lett. 473, 205–214. https://doi.org/10.1016/j.epsl.2017.06.011.
McColl, S.T., 2012. Paraglacial rock-slope stability. Geomorphology 153–154, 1–16. https://doi.org/10.1016/j.geomorph.2012.02.015.
Menéndez-Duarte, R., Fernández, F.J., 2014. Avalanchas calcáreas en el arco externo de la Sierra de la Sobia (Zona Cantábrica, NO Iberia) desencadenadas por la reactivación de la Falla de León: XIII Reunión Nacional de Geomorfología. Cáceres 2014, 397–400.
Merchel, S., Bremser, W., Alfimov, V., Arnold, M., Aumaître, G., Benedetti, L., Bourlès, D. L., Caffee, M., Fifield, L.K., Finkel, R.C., Freeman, S.P.H.T., Martschini, M., Matsushi, Y., Rood, D.H., Sasa, K., Steier, P., Takahashi, T., Tamari, M., Tims, S.G., Tosaki, Y., Wilcken, K.M., Xu, S., 2011. Ultra-trace analysis of 36Cl by accelerator mass spectrometry: An interlaboratory study. Anal. Bioanal. Chem. 400, 3125–3132. https://doi.org/10.1007/s00216-011-4979-2.
Mercier, D., Coquin, J., Feuillet, T., Decaulne, A., Cossart, E., Jónsson, H.P., Sæmundsson, Þ., 2017. Are Icelandic rock-slope failures paraglacial? Age evaluation of seventeen rock-slope failures in the Skagafjörður area, based on geomorphological stacking, radiocarbon dating and tephrochronology. Geomorphology 296, 45–58. https://doi.org/10.1016/j.geomorph.2017.08.011.
Merino-Tomé, O., Suárez, Á., Alonso, J.L., González-Menéndez, L., Heredia, N., Marcos-Vallaure, A., 2011. Mapa Geológico Digital continuo E. 1:50000, Principado de Asturias (Zonas: 1100-1000-1600) , in: Navas, J. (Ed.), GEODE. Mapa Geológico Digital Continuo de España. Sistema de Información Continua: SIGECO. IGME, Madrid.
Moore, J.R., Gischig, V., Burjanek, J., Loew, S., Fäh, D., 2011. Site Effects in Unstable Rock Slopes: Dynamic Behavior of the Randa Instability (Switzerland). Bull. Seismol. Soc. Am. 101, 3110–3116. https://doi.org/10.1785/0120110127.
Nagelisen, J., Moore, J.R., Vockenhuber, C., Ivy-Ochs, S., 2015. Post-glacial rock avalanches in the Obersee Valley, Glarner Alps, Switzerland. Geomorphology 238, 94–111. https://doi.org/10.1016/j.geomorph.2015.02.031.
Nicolussi, K., Spötl, C., Thurner, A., Reimer, P.J., 2015. Precise radiocarbon dating of the giant Köfels landslide (Eastern Alps, Austria). Geomorphology 243, 87–91. https://doi.org/10.1016/j.geomorph.2015.05.001.
Oswald, P., Moernaut, J., Fabbri, S.C., De Batist, M., Hajdas, I., Ortner, H., Titzler, S., Strasser, M., 2021a. Combined On-Fault and Off-Fault Paleoseismic Evidence in the Postglacial Infill of the Inner-Alpine Lake Achensee (Austria, Eastern Alps). Front. Earth Sci. 9, 1–25. https://doi.org/10.3389/feart.2021.670952.
Oswald, P., Strasser, M., Hammerl, C., Moernaut, J., 2021b. Seismic control of large prehistoric rockslides in the Eastern Alps. Nat. Commun. 12, 1–8. https://doi.org/10.1038/s41467-021-21327-9.
Pedreira, D., Afonso, J.C., Pulgar, J.A., Gallastegui, J., Carballo, A., Fernàndez, M., Garcia-Castellanos, D., Jiménez-Munt, I., Semprich, J., García-Moreno, O., 2015. Geophysical-petrological modeling of the lithosphere beneath the Cantabrian Mountains and the North-Iberian margin: geodynamic implications. Lithos 230, 46–68. https://doi.org/10.1016/j.lithos.2015.04.018.
Pedreira, D., Pulgar, J.A., Gallart, J., Díaz, J., 2003. Seismic evidence of Alpine crustal thickening and wedging from the western Pyrenees to the Cantabrian Mountains (north Iberia). J. Geophys. Res. Solid Earth 108, n/a-n/a. https://doi.org/10.1029/2001jb001667.
Pedreira, D., Pulgar, J.A., Gallart, J., Torné, M., 2007. Three-dimensional gravity and magnetic modeling of crustal indentation and wedging in the western Pyrenees-Cantabrian Mountains. J. Geophys. Res. 112 https://doi.org/10.1029/2007jb005021.
Pérez-Alberti, A., Valcárcel-Díaz, M., Blanco-Chao, R., 2004. Pleistocene glaciation in Spain. In: Ehlers, J., Gibbard, P.L. (Eds.), Quaternary Glaciations - Extent and Chronology. Elsevier, pp. 388–394.
Pulgar, J.A., Alonso, J.L., Espina, R.G., Marín, J.A., 1999. La deformación alpina en el basamento varisco de la Zona Cantábrica. Trab. Geol. 21, 283–294.
Rodríguez-Pérez, C., 2012. La evolución antigua del relieve en el área central de la Cordillera Cantábrica. Eria 89, 203–230.
Rodríguez-Rodríguez, L., González-Lemos, S., Ballesteros, D., Valenzuela, P., Domínguez-Cuesta, M.J., Llana-Fúnez, S., Jiménez-Sánchez, M., 2018. Timing of paraglacial rock-slope failures and denudation signatures in the Cantabrian Mountains (North Iberian Peninsula). L. Degrad. Dev. 29, 3159–3173. https://doi.org/10.1002/ldr.3012.
Santos-González, J., Redondo-Vega, J.M., González-Gutiérrez, R.B., Gómez-Villar, A., 2013. Applying the AABR method to reconstruct equilibrium-line altitudes from the last glacial maximum in the Cantabrian Mountains (SW Europe). Palaeogeogr. Palaeoclimatol. Palaeoecol. 387, 185–199. https://doi.org/10.1016/j.palaeo.2013.07.025.
Schimmelpfennig, I., Benedetti, L., Finkel, R., Pik, R., Blard, P.H., Bourlès, D., Burnard, P., Williams, A., 2009. Sources of in-situ 36Cl in basaltic rocks. Implications for calibration of production rates. Quat. Geochronol. 4, 441–461. https://doi.org/10.1016/j.quageo.2009.06.003.
Stich, D., Martínez-solares, J.M., Custódio, S., Batlló, J., Martín, R., Teves-costa, P., Morales, J., 2020. Seismicity of the Iberian Peninsula. In: Quesada, C., Oliveira, J. (Eds.), The Geology of Iberia: A Geodynamic Approach. Springer International Publishing, pp. 11–32. https://doi.org/10.1007/978-3-030-10931-8.
Stock, G.M., Uhrhammer, R.A., 2010. Catastrophic rock avalanche 3600 years BP from el Capitan, Yosemite Valley, California. Earth Surf. Process. Landforms 35, 941–951. https://doi.org/10.1002/esp.1982.
Stoll, H.M., Moreno, A., Mendez-Vicente, A., Gonzalez-Lemos, S., Jimenez-Sanchez, M., Dominguez-Cuesta, M.J., Edwards, R.L., Cheng, H., Wang, X., 2013. Paleoclimate and growth rates of speleothems in the northwestern Iberian Peninsula over the last two glacial cycles. Quat. Res. 80, 284–290. https://doi.org/10.1016/j.yqres.2013.05.002.
Stone, J., 2000. Air pressure and cosmogenic isotope production. J. Geophys. Res. 105, 23753–23759.
Storti, F., Billi, A., Salvini, F., 2003. Particle size distributions in natural carbonate fault rocks: Insights for non-self-similar cataclasis. Earth Planet. Sci. Lett. 206, 173–186. https://doi.org/10.1016/S0012-821X(02)01077-4.
Thomas, E.R., Wolff, E.W., Mulvaney, R., Steffensen, J.P., Johnsen, S.J., Arrowsmith, C., White, J.W.C., Vaughn, B., Popp, T., 2007. The 8.2 ka event from Greenland ice cores. Quat. Sci. Rev. 26, 70–81. https://doi.org/10.1016/j.quascirev.2006.07.017.
Villa, E., de Sánchez Posada, L.C., Fernández, L.P., Martínez-Chacón, M.L., Stavros, C., 2001. Foramanifera and biostratigraphy of the Valdeteja Formation stratotype (Carboniferous, Cantabrian Zone, NW Spain). Facies 45, 59–86. https://doi.org/10.1007/BF02668105.

Villamor, P., Capote, R., Stirling, M.W., Tsige, M., Berryman, K.R., Martínez-Díaz, J.J., Martín-González, F., 2012. Contribution of active faults in the intraplate area of Iberia to seismic hazard: The Alentejo-Plasencia Fault. J. Iber. Geol. 38, 85–111. https://doi.org/10.5209/rev_jige.2012.v38.n1.39207.

Wagner, R.H., Winkler Prins, C.F., Riding, R.E., 1971. Lithostratigraphic units of the lower part of the Carboniferous in Northern León. Spain. Trab. Geol. 4, 603–663.

Yin, Y., Sun, P., Zhu, J., Yang, S., 2011. Research on catastrophic rock avalanche at Guanling, Guizhou, China. Landslides 8, 517–525. https://doi.org/10.1007/s10346-011-0266-8.

Zerathe, S., Lebourg, T., Braucher, R., Bourlès, D., 2014. Mid-Holocene cluster of large-scale landslides revealed in the Southwestern Alps by 36Cl dating. Insight on an Alpine-scale landslide activity. Quat. Sci. Rev. 90, 106–127. https://doi.org/10.1016/j.quascirev.2014.02.015.

Zhou, Z.H., Lyu, Y., Su, S., rui, Liu, S. jie, Zhao, H., Li, P., Zhou, Y.,, 2020. Characteristics and dynamics of the Ganqiuchi rock avalanche triggered by a paleo-earthquake in the Northern Qinling Mountains. J. Mt. Sci. 17, 1143–1160. https://doi.org/10.1007/s11629-019-5599-0.

Zreda, M.G., Phillips, F.M., Elmore, D., Kubik, P.W., Sharma, P., Dorn, R.I., 1991. Cosmogenic chlorine-36 production rates in terrestrial rocks. Earth Planet. Sci. Lett. 105, 94–109. https://doi.org/10.1016/0012-821X(91)90123-Y.